Improving lung cancer treatment: Hyaluronic acid-modified and glutathione-responsive amphiphilic TPGS-doxorubicin prodrug-entrapped nanoparticles

GUOJUN LU[1*], LEI CAO[2*], CHENYAO ZHU[3], HAIYAN XIE[1], KEKE HAO[1], NING XIA[1], BO WANG[2], YU ZHANG[1] and FENG LIU[2]

Departments of [1]Respiratory Medicine and [2]Thoracic Surgery, Nanjing Chest Hospital, School of Medicine, Southeast University, Nanjing, Jiangsu 210029; [3]Shenzhen Yuce Biotechnology Co. Ltd, Shenzhen, Guangdong 518000, P.R. China

Received November 27, 2018; Accepted April 12, 2019

DOI: 10.3892/or.2019.7139

Abstract. Lung cancer nanotherapeutics aim to overcome the limitations of conventional therapeutic methods. In the present study, a self-assembled amphiphilic prodrug-based nanocarrier delivery system was developed that exhibited high therapeutic efficiency. D-alpha-tocopheryl polyethylene glycol 1000 succinate (TPGS) conjugated to doxorubicin (DOX) through disulfide (S-S) bonds to constitute TPGS-S-S-DOX was synthesized; furthermore, hyaluronic acid (HA) was conjugated to TPGS to obtain HA-TPGS. TPGS-S-S-DOX prodrug-based and HA-TPGS ligand-modified nanoparticles (HA-TPGS DOX-NPs) were prepared for the treatment of lung cancer. *In vitro* and *in vivo* evaluation of the system was performed on lung cancer cell lines and lung tumor-bearing mice. HA-TPGS DOX-NPs had a uniformly spherical shape with a white core and grey shell, with a size of 172.3 nm and a polydispersity index of 0.16. All of the NPs exhibited a drug encapsulation efficiency of >90%. The blank NPs exhibited low toxicity to all the tested cell lines, resulting in viabilities of >85%. HA-TPGS DOX-NPs had a more prominent *in vitro* antitumor effect than the other NPs tested, with cell viabilities of 80.2, 73.4, 57.8, 39.1, 28.3 and 10.9% observed after 72 h of incubation with 0.01, 0.05, 0.1, 0.5, 1 and 5 μM, respectively. The *in vivo* results demonstrated that HA-TPGS DOX-NPs had the highest antitumor efficacy, with 10.5% tumor inhibition efficiency after 28 days of injection. Overall, HA-TPGS DOX-NPs had significant antitumor effects and minimal systemic toxicity, and their application may be a promising strategy for the treatment of lung cancer.

Correspondence to: Dr Yu Zhang, Department of Respiratory Medicine, Nanjing Chest Hospital, School of Medicine, Southeast University, 215 Guangzhou Road, Nanjing, Jiangsu 210029, P.R. China
E-mail: zhangyu2113-nj@163.com

Dr Feng Liu, Department of Thoracic Surgery, Nanjing Chest Hospital, School of Medicine, Southeast University, 215 Guangzhou Road, Nanjing, Jiangsu 210029, P.R. China
E-mail: liufengseu@sohu.com

[*]Contributed equally

Key words: lung cancer, prodrug-based nanocarriers, hyaluronic acid, doxorubicin, ligand-modified nanoparticles,

Introduction

Lung cancer is the major cause of cancer-associated mortality worldwide (1). Lung cancer nanotherapeutics is a strategy to overcome the limitations of the conventional methods available for diagnosis and treatment (2). Nanoparticle (NP) systems have improved the chemotherapeutic efficiency of drugs associated with poor solubility, stability or adverse effects on their own by providing different pathways. The lipid prodrug strategy is one of the promising methods involving NP systems (3). The advantages of lipid-based prodrug nanocarriers include improved drug encapsulation and stability, balancing of the pharmacokinetics of drugs, controlled drug release and enhanced biocompatibility (4).

D-alpha-tocopheryl polyethylene glycol 1000 succinate (TPGS), a water-soluble derivative of natural vitamin E, has an amphiphilic structure comprised of a lipophilic alkyl tail and a hydrophilic polar head portion (5). It has already demonstrated advantages when applied along with various anticancer drugs, e.g. doxorubicin (DOX), including enhanced therapeutic effects and reduced side effects (6). Tumor cells contain a higher concentration of glutathione (GSH, 2-8 mM) than normal cells (7). Numerous disulfide-based proteins and small-molecule prodrug strategies have been developed that rely on high intracellular GSH levels (8). Furthermore, active transport of activated disulfides into cells is increasingly recognized as an important mechanism for cell delivery. Disulfide (S-S) bonds may be rapidly cleaved by intracellular GSH, following which intracellular targeting may be achieved (9). In addition, through the disulfide bond connection, the self-assembly and stabilization of hydrophobic prodrugs are supported (10). In the present study, TPGS was conjugated to DOX through S-S bonds to constitute TPGS-S-S-DOX.

Hyaluronic acid (HA) is a natural line polysaccharide. Due to its high affinity toward CD44, a cell adhesion membrane glycoprotein overexpressed on the surface of cancer cells, HA has high tumor-specific targeting properties to (lung) cancer cells compared to normal cells (11). HA is not only a structural component of the extracellular matrix of the tumor cell but also a biologically active molecule that may promote tumor progression through induction of cell signaling (12). In addition, HA protects tumor tissues against immune surveillance and chemotherapeutic agents. In the present study, HA was conjugated to TPGS to obtain HA-TPGS.

Self-assembled amphiphilic prodrug-based nanocarrier delivery systems may overcome the limitations of common prodrugs, which on their own may be chemically or enzymatically degraded *in vivo* in an uncontrolled manner (13). Combining the advantages of prodrug and nanomedicine strategies in cancer therapy may achieve high therapeutic efficiency. In the present study, the advantages of prodrug and nanomedicine strategies were combined and a self-assembled TPGS-S-S-DOX prodrug-based and HA-TPGS ligand-containing nanomedicine (HA-TPGS DOX-NPs) was developed for the treatment of lung cancer. *In vitro* and *in vivo* evaluation of the system were performed using lung cancer cell lines and lung tumor-bearing mice, respectively.

Materials and methods

Chemicals and reagents. TPGS was obtained from Eastman Chemical Co. (Kingsport, TN, USA). TPGS-COOH was synthesized according to previous studies (14,15). HA (molecular weight, 7.8 kDa) was purchased from Freda Biochem Co., Ltd. (Linyi, China). HA-TPGS was synthesized according to a previous study (16). Polylactic acid (PLA) was purchased from Jinan Daigang Biomaterial Co., Ltd. (Jinan, China). DOX, DMSO, 1-ethyl-3-(3-dimethylaminopropyl) carbodiimide (EDC), N-hydroxysuccinimide (NHS), Dulbecco's modified Eagle's medium (DMEM), fetal bovine serum (FBS), Tween®-80 and MTT were obtained from Sigma-Aldrich (Merck KGaA, Darmstadt, Germany).

Cell lines and culture. The A549 and HCC827 lung cancer cell lines and the MRC-5 human embryonic lung cell line were obtained from the American Type Culture Collection and cultured in DMEM and RPMI-1640 medium, respectively, supplemented with 10% (v/v) FBS, 1% non-essential amino acids, 1% L-glutamine and 1% streptomycin-penicillin (100 IU/ml) at 37˚C, in a humidified atmosphere of 95% air and 5% CO_2 (17).

Animal model. HCC827 cells ($1x10^6$ cells/animal) were injected into the lateral tail vein of 4- to 6-week-old, female BALB/c nude mice (100 mice; Shandong University Laboratory Animal Center, Jinan, China) to produce a lung cancer-bearing animal model (18), mice were raised under conventional conditions with a 12 h light/dark cycle, constant temperature (25˚C) and humidity (60%) with access to food and water *ad libitum*. The animal experiments complied with the Guide for the Care and Use of Laboratory Animals of the National Institutes of Health (publication no. 8023; Bethesda, MD, USA) and approval was obtained from the Institutional Animal Care and Treatment Committee of Southeast University (Nanjing, China). A loss of >20% of body weight; mice that could not take in food for 24 h; who could not stand for 24 h; whose tumor weight exceeded 10% of their body weight; or whose average tumor diameter was >20 mm were set as humane endpoints of the animal experiments.

Synthesis of TPGS-S-S-DOX. The TPGS-S-S-DOX prodrug was synthesized as follows (Fig. 1): TPGS-COOH was dissolved in DMSO, EDC·HCl (1.2 equivalents) and NHS (1.2 equivalents) were added, followed by stirring for 2 h at room temperature (RT). 2,2'-Dithiodibenzoic acid (1 equivalent) was added to TPGS-COOH and the mixture was stirred for 20 h at RT to yield TPGS-S-S. Glutamic acid (GA) was dissolved in DMSO, and EDC·HCl (1.2 equivalents) and NHS (1.2 equivalents) were added, followed by stirring for 2 h at RT. TPGS-S-S was added to GA and stirred for 20 h at RT to yield TPGS-S-S-GA. TPGS-S-S-DOX as obtained by dissolving TPGS-S-S-GA in DMSO with added EDC·HCl (1.2 equivalents) and NHS (1.2 equivalents), and DOX (dissolved in DMSO) was then added to this mixture, which was stirred for 20 h at RT. TPGS-S-S-DOX was dialyzed against water for 24 h and lyophilized. The chemical structure of TPGS-S-S-DOX was confirmed using ^{1}H-nuclear magnetic resonance (NMR) analysis.

Self-assembly of HA-TPGS DOX-NPs. Self-assembled HA-TPGS DOX-NPs (Fig. 2) were prepared via a dialysis method (19,20). In brief, 100 mg TPGS-S-S-DOX and 100 mg PLA were dissolved in 10 ml DMSO, to which 20 ml HA-TPGS (100 mg) and Tween®-80 (1%) in deionized water was added dropwise to obtain the self-assembled HA-TPGS DOX-NPs mixture. The mixture was subsequently transferred to a dialysis bag [molecular weight cut-off (MWCO), 10,000 Da] and dialyzed against distilled water for 48 h. Blank (DOX-free) HA-TPGS-containing NPs (HA-TPGS NPs) were prepared by the same method using TPGS-S-S without the presence of DOX. DOX-containing NPs without the HA ligand modification (TPGS DOX-NPs) were manufactured with the same method using TPGS without the presence of HA. DOX-loaded PLA NPs (DOX-NPs) lacking HA-TPGS were also prepared by the same method using DOX without TPGS and S-S. The final products were harvested after lyophilization.

Characterization of HA-TPGS DOX-NPs. One drop of HA-TPGS DOX-NPs, TPGS DOX-NPs or DOX-NPs was dissolved in PBS (1 mg/ml) separately, and was carefully cast onto a clean copper grid (21). Subsequently, extra solution was air-dried and directly observed under a transmission electron microscope (TEM) without staining. The morphology of HA-TPGS DOX-NPs, TPGS DOX-NPs or DOX-NPs was examined using a TEM (JEM-1200EX; JEOL, Ltd., Tokyo, Japan), operated at an acceleration voltage of 100 kV.

The dynamic light scattering (DLS) method was applied to determine the particle size, polydispersity index (PDI) and zeta potential (ZP) of NPs using a Zetasizer® Nano-ZS90 (Malvern Instruments, Malvern, UK) (22).

For evaluation of drug encapsulation efficiency (EE) and drug-loading content (DL), HA-TPGS DOX-NPs was passed through an ultrafiltration tube (MWCO, 10,000 Da) at 15,930 x g for 30 min (23). The amount of DOX in the

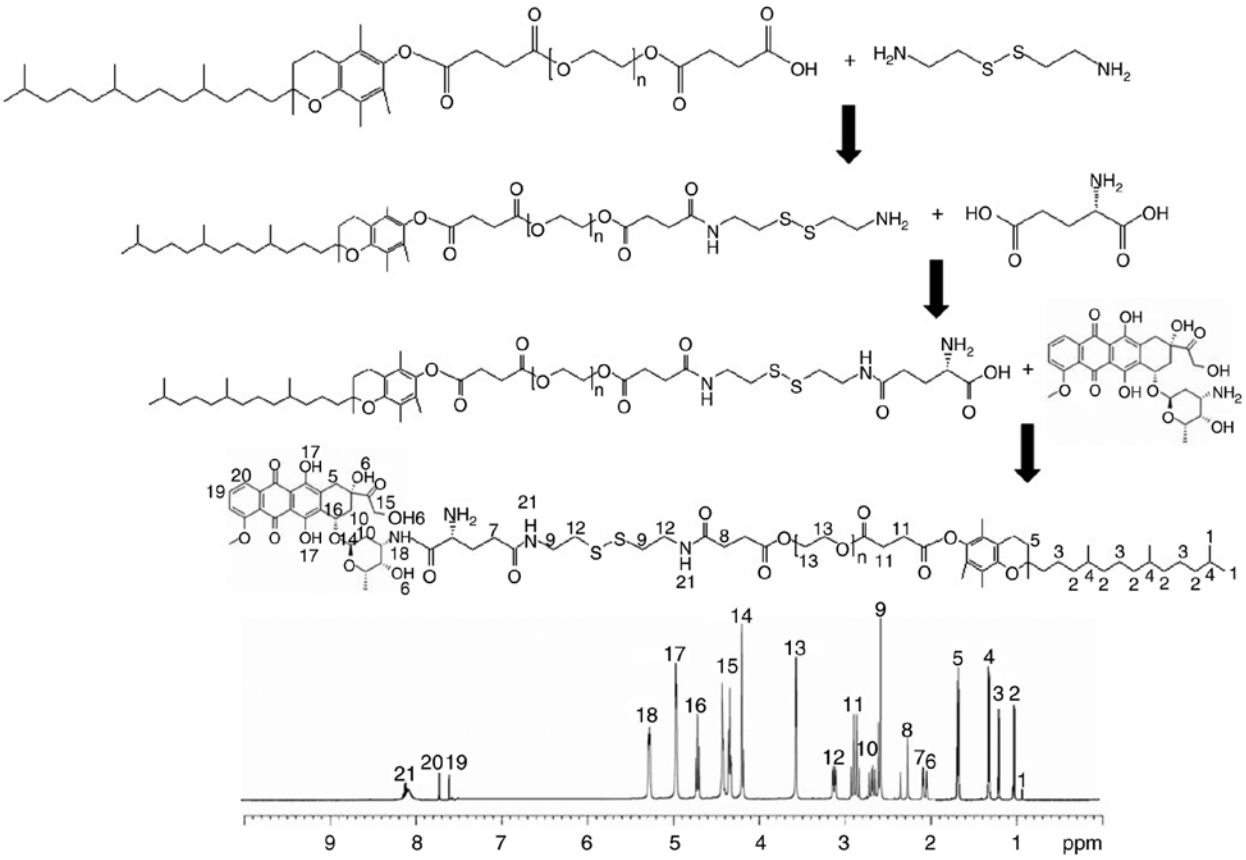

Figure 1. Synthesis scheme and ^{1}H-NMR spectrum of the TPGS-S-S-DOX prodrug. TPGS-COOH was conjugated with 2,2'-dithiodibenzoic acid to yield TPGS-S-S. PGS-S-S was added to GA to yield TPGS-S-S-GA. TPGS-S-S-DOX as obtained by conjugating TPGS-S-S-GA along with DOX. The chemical structure of TPGS-S-S-DOX was confirmed using ^{1}H-NMR analysis. NMR, nuclear magnetic resonance; TPGS, D-alpha-tocopheryl polyethylene glycol 1000 succinate; DOX, doxorubicin; GA, glutamic acid.

filtrate was assessed by detecting the UV absorbance at the wavelength of 480 nm using an UV-1201 spectrophotometer (Shimadzu Corporation, Kyoto, Japan) (24).

The stability of NPs in the presence of serum was examined by incubation with 10% FBS (25). HA-TPGS DOX-NPs, HA-TPGS NPs, TPGS DOX-NPs or DOX-NPs were incubated with 10% FBS (v/v) solution at 37˚C with gentle stirring at 100 rpm for 1, 2, 4, 8, 24, 48 or 72 h. At each time-point, the NPs were centrifuged at 67 x g for 10 min. Their size and PDI were then measured.

In vitro drug release. The dialysis bag method was used to assess the *in vitro* release of HA-TPGS DOX-NPs in comparison with TPGS DOX-NPs and DOX-NPs (26). Of the samples, 10 ml were placed into dialysis bags (MWCO, ~14,000), which were then sealed and dialyzed against 100 ml PBS (pH 7.4, 37˚C). A total of 200 μl release medium was withdrawn at pre-determined intervals (0, 2, 4, 8, 16, 24, 48, 72, 96 and 120 h) and immediately replaced with the same volume of fresh medium to maintain sink conditions. The amount of drug released was analyzed by the same method as in that in the aforementioned section and the release curves were plotted.

Cellular uptake assay. Coumarin 6, which may be encapsulated into various NPs for quantitative investigation of cellular uptake (27), was used in the present study as a model fluorescent molecule to evaluate cellular uptake efficiency of NPs. Coumarin 6 was encapsulated into the HA-TPGS DOX-NPs, HA-TPGS NPs, TPGS DOX-NPs or DOX-NPs by the same synthetic method as that stated above, and a total of 50 mg coumarin 6 was added along with the PLA (28). A549 and HCC827 cells were seeded in 24-well culture plates ($5x10^4$ cells/well) and incubated for 24 h (37˚C). After the cells reached ~80% confluence, different NPs were added to replace the medium, followed by incubation for 2, 4 or 8 h. Subsequently, the cells were washed three times with D-Hank's solution, collected and centrifugated (15,93 x g, 5 min), and the fluorescence of cells was analyzed using a flow cytometer.

In vitro cytotoxicity of NPs. The *in vitro* cytotoxicity of HA-TPGS NPs was evaluated by measuring the viability of cells treated with different concentrations of NPs using an MTS assay (29). A549, HCC827 and MRC-5 cells ($5x10^4$ cells/ml in 200 μl) were seeded separately into 96-well plates and incubated for 24 h. HA-TPGS NPs at different concentrations were added, followed by incubation for 72 h. The cell viability was evaluated with a CellTiter 96® AQueous One Solution Reagent (Promega Corporation, Madison, WI, USA). Cell culture medium (100 μl) was supplemented with fresh medium with MTS (20 μl/well). The cell viability was calculated using the following equation: Cell viability (%)=(absorbance of treatment group)/(absorbance of control group) x100. Culture medium only served as a negative control.

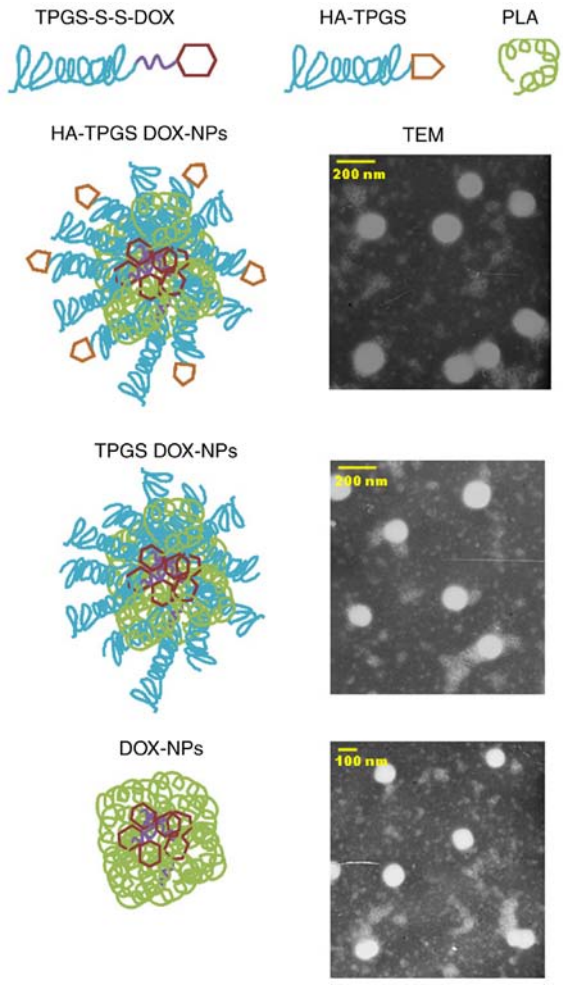

Figure 2. Scheme graph and surface morphologies of HA-TPGS DOX-NPs. Self-assembled HA-TPGS DOX-NPs were prepared by a dialysis method. The morphology of HA-TPGS DOX-NPs, TPGS DOX-NPs and DOX-NPs was examined using a transmission electron microscope (JEM-1200EX; JEOL), operated at an acceleration voltage of 100 kV. TPGS, D-alpha-tocopheryl polyethylene glycol 1000 succinate; DOX, doxorubicin; HA, hyaluronic acid; NP, nanoparticle.

In vitro anticancer efficacy. The *in vitro* anticancer efficacy of NPs was assessed by determining the inhibition efficiency on A549 and HCC827 cells using the same method as aforementioned. The only difference was that DOX-loaded NPs and free DOX at different concentrations were added instead of HA-TPGS NPs (30).

In vivo antitumor efficiency. A lung cancer-bearing animal model was prepared by injecting HCC827 cells ($1x10^6$ cells/mouse) into the lateral tail vein of BALB/c nude mice as mentioned in the '*Animal model*' section. After 1 week, mice with tumors (volume of 100 mm^3) were randomly divided into 6 groups (8 mice per group) that were respectively injected with 0.2 ml of i) HA-TPGS DOX-NPs; ii) HA-TPGS NPs; iii) TPGS DOX-NPs; iv) DOX-NPs; and v) free DOX (equivalent DOX concentration, 10 mg/kg) or vi) 0.9% saline solution via the tail vein on days 0, 4, 8 and 12 (31). The tumors were measured every 4 days with a Vernier caliper and the volumes were calculated using the following equation: Tumor volume (mm^3)=(largest diameter) x (smallest diameter) x (height of the tumor)/2. The antitumor efficacy of the drugs/NPs was evaluated by calculating the tumor inhibition rate (TIR) according to the following equation: TIR (%)=(tumor weight of the negative control group-tumor weight of the treatment group)/(tumor weight of the negative control group) x100 (32). Images of the tumors were captured at the end of the study. Body weight changes were monitored in order to evaluate the systemic toxicity of the drugs/NPs.

Statistical analysis. Values are expressed as the mean ± standard deviation. Statistical significances were evaluated using one-way analysis of variance (ANOVA) followed by Tukey's test for multiple comparisons. $^{*}P<0.05$, $^{**}P<0.01$ was considered to indicate a statistically significant difference.

Results

Characterization of TPGS-S-S-DOX. To confirm the formation of TPGS-S-S-DOX, ^{1}H-NMR analyses were performed, and the spectra are provided in Fig. 1. The peaks, including those for the TPGS protons, e.g. $-CH_2-$ and $-CH_3$ at 0.9-1.7 ppm (peaks, 1-5), the protons of PEG at 3.6 ppm (peak, 13), the-S-S-unit at 2.5-3.2 ppm (peaks, 9-12), as well as the protons of DOX at 4.2-7.8 (peaks, 14-20), confirmed the presence of TPGS, S-S and DOX. The peaks at 7, 8, 9, 12 and 21 illustrated the covalent conjugation of the materials through amide linkages.

Characterization of HA-TPGS DOX-NPs. TEM revealed the surface morphology and particle size of HA-TPGS DOX-NPs (Fig. 2). The image indicates that HA-TPGS DOX-NPs had a uniformly spherical shape with a white core and grey shell. The NPs had a size of <200 nm. These results are in agreement with the particle size and PDI determination (Table I). HA-TPGS DOX-NPs had a size of 172.3 nm and a PDI of 0.16. All of the NPs exhibited a negative ZPs and EEs of >90%. The stability of HA-TPGS DOX-NPs was evaluated in the presence of 10% FBS at 37˚C for 72 h. HA-TPGS DOX-NPs, TPGS DOX-NPs or DOX-NPs in a solution with 10% FBS exhibited no significant changes in size or PDI (Fig. 3).

In vitro drug release. The release profiles of the NPs are presented in Fig. 4. The release of drug from DOX-NPs was faster than that from HA-TPGS DOX-NPs and TPGS DOX-NPs ($P<0.05$). The release of DOX from DOX-NPs reached 90% within 48 h, compared with 96 h for HA-TPGS DOX-NPs and TPGS DOX-NPs, indicating a more sustained drug release behavior of the modified NPs. The most sustained release pattern observed for HA-TPGS DOX-NPs may be attributed to the coating of HA and TPGS that made the release of the drug slower.

Cellular uptake assay. As indicated in Fig. 5, the uptake of NPs into A549 and HCC827 cells was increased with time from 2 to 8 h. The cellular uptake efficiency of the HA-modified HA-TPGS DOX-NPs and HA-TPGS NPs was markedly higher than that of other NPs, reaching >80% at 8 h in either of the two cell lines ($P<0.01$). The cellular uptake of TPGS DOX-NPs was markedly higher than that of DOX-NPs at 4 and 8 h ($P<0.05$).

Table I. Physicochemical characteristics of NPs (mean ± SD, n=3).

Formulation	Size (nm)	PDI	ZP (mV)	EE (%)	DL (%)
HA-TPGS DOX-NPs	172.3±6.5	0.16±0.04	-39.5±3.3	90.2±2.8	7.6±0.3
HA-TPGS NPs	170.9±5.4	0.12±0.05	-33.7±2.9	N/A	N/A
TPGS DOX-NPs	133.6±5.2	0.13±0.05	-26.3±2.5	91.4±3.1	9.2±0.5
DOX-NPs	102.4±4.2	0.11±0.03	-18.2±1.6	90.9±2.3	15.3±0.9

PDI, polydispersity index; ZP, zeta potential; EE, encapsulation efficiency; DL, drug loading content; TPGS, D-alpha-tocopheryl polyethylene glycol 1000 succinate; DOX, doxorubicin; HA, hyaluronic acid; NPs, nanoparticles.

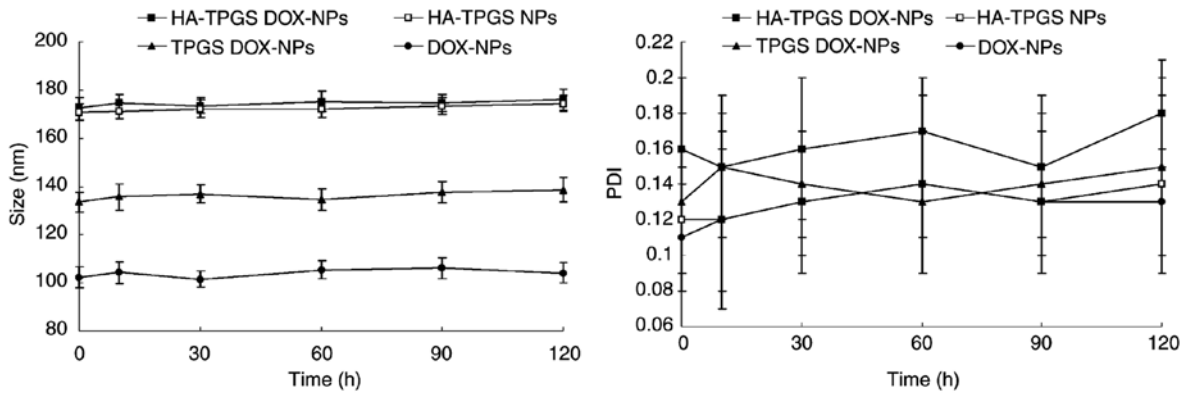

Figure 3. Stability of HA-TPGS DOX-NPs evaluated in the presence of serum. HA-TPGS DOX-NPs, HA-TPGS NPs, TPGS DOX-NPs or DOX-NPs were incubated with 10% fetal bovine serum (v/v) at 37˚C with gentle stirring at 100 rpm for 1, 2, 4, 8, 24, 48 or 72 h. At each time-point, the NPs were centrifuged at 67 x g for 10 min. Their size and polydispersity index were measured. Values are expressed as the mean ± standard deviation (n=3). TPGS, D-alpha-tocopheryl polyethylene glycol 1000 succinate; DOX, doxorubicin; HA, hyaluronic acid; NP, nanoparticle.

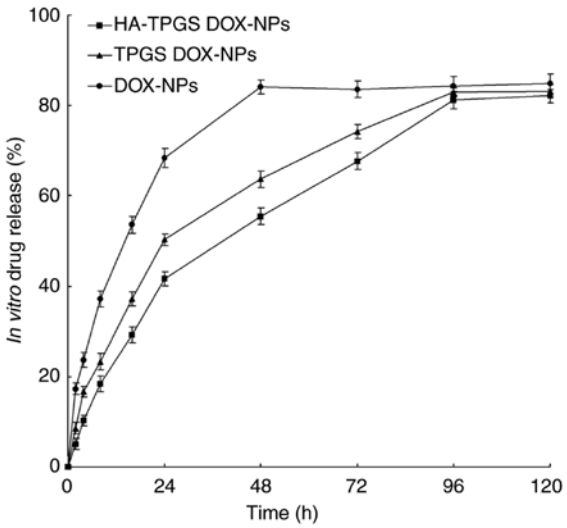

Figure 4. *In vitro* release of drugs by NPs. HA-TPGS DOX-NPs, TPGS DOX-NPs and DOX-NPs (10 ml) were placed into the dialysis bags (molecular weight cut-off, ~14,000) separately, sealed and dialyzed against 100 ml PBS (pH 7.4, 37˚C). Values are expressed as the mean ± standard deviation (n=3). TPGS, D-alpha-tocopheryl polyethylene glycol 1000 succinate; DOX, doxorubicin; HA, hyaluronic acid; NP, nanoparticle.

In vitro cytotoxicity. Table II presents the *in vitro* cytotoxicity data of blank HA-TPGS NPs on A549, HCC827 and MRC-5 cells at different concentrations. The cell viability decreased along with the increase in the NP concentration. Considering that the cell viability was >85% in all groups, the NP system should be regarded as having low toxicity and good biocompatibility.

In vitro anticancer efficiency. As indicated in Fig. 6, the cell inhibitory effects of DOX-loaded NPs were significantly higher than those of free DOX (P<0.05). HA-TPGS DOX-NPs exhibited a significantly greater cytotoxicity than the other NPs tested (P<0.05), and cell viabilities of 80.2, 73.4, 57.8, 39.1, 28.3 and 10.9% were measured after 72 h of incubation with DOX-NPs with equivalent DOX concentrations of 0.01, 0.05, 0.1, 0.5, 1 and 5 μM, respectively. Notably, the inhibitory effect of DOX-loaded NPs on HCC827 cells was greater than that on A549 cells.

In vivo antitumor efficiency. As presented in Fig. 7, the tumor volume of the mice treated with 0.9% saline control or blank HA-TPGS NPs increased rapidly along with time and the tumor growth curves were similar among these groups. Notably, the tumor growth was effectively inhibited in all DOX-loaded NP groups and slightly inhibited by free DOX (P<0.05). The TPGS DOX-NPs exhibited a greater tumor growth inhibition efficiency compared with that of DOX-NPs (P<0.05). The HA-TPGS DOX-NPs had a more significant tumor suppression ability in comparison to the other groups (P<0.01); after 28 days, the TIR of HA-TPGS DOX-NPs, TPGS DOX-NPs, DOX-NPs and free DOX was 78.7, 55.4, 28.2 and 10.5%, respectively. The physical activity level and body weight of

Table II. Cytotoxicity evaluation of blank HA-TPGS NPs at different concentrations (mean ± SD, n=6).

Concentration (μM) (%)	10	5	1	0.5	0.1
A549 cell viability	86.9±3.7	88.4±2.9	90.1±2.6	93.2±2.9	94.1±2.2
HCC827 cell viability	85.1±4.1	87.9±3.5	89.2±3.1	90.12±2.6	91.6±2.5
MRC-5 cell viability	90.1±2.9	91.5±3.1	92.3±3.5	91.6±3.1	94.6±2.7

TPGS, D-alpha-tocopheryl polyethylene glycol 1000 succinate; HA, hyaluronic acid; NPs, nanoparticles.

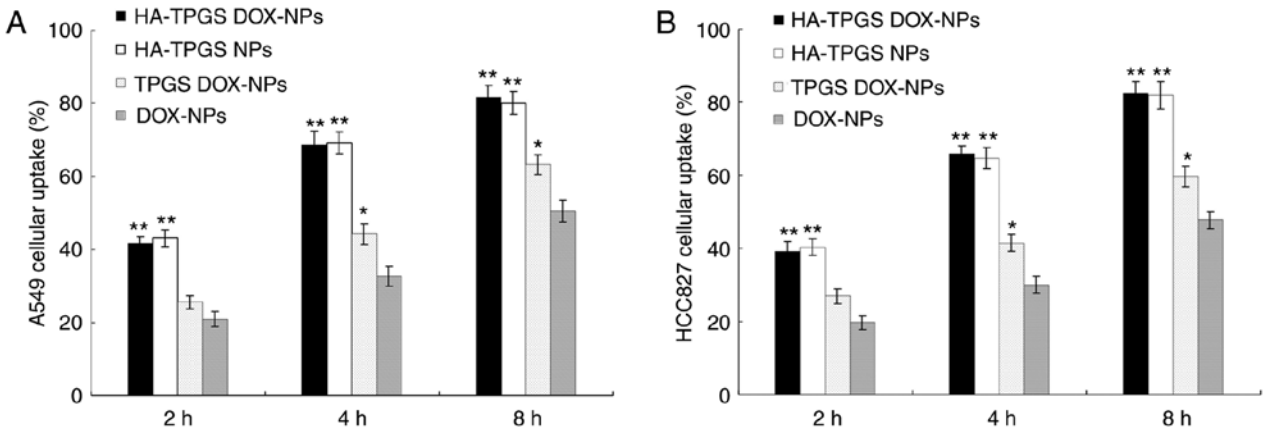

Figure 5. Cellular uptake efficiency of NPs into (A) A549 and (B) HCC827 cells at 2-8 h. Coumarin 6 was loaded in the HA-TPGS DOX-NPs, HA-TPGS NPs, TPGS DOX-NPs or DOX-NPs, and they were incubated with A549 and HCC827 cells. The fluorescence of cells was analyzed using a flow cytometer. Values are expressed as the mean ± standard deviation (n=3). *P<0.05 vs. DOX-NPs; **P<0.01 vs. DOX-NPs. TPGS, D-alpha-tocopheryl polyethylene glycol 1000 succinate; DOX, doxorubicin; HA, hyaluronic acid; NP, nanoparticle.

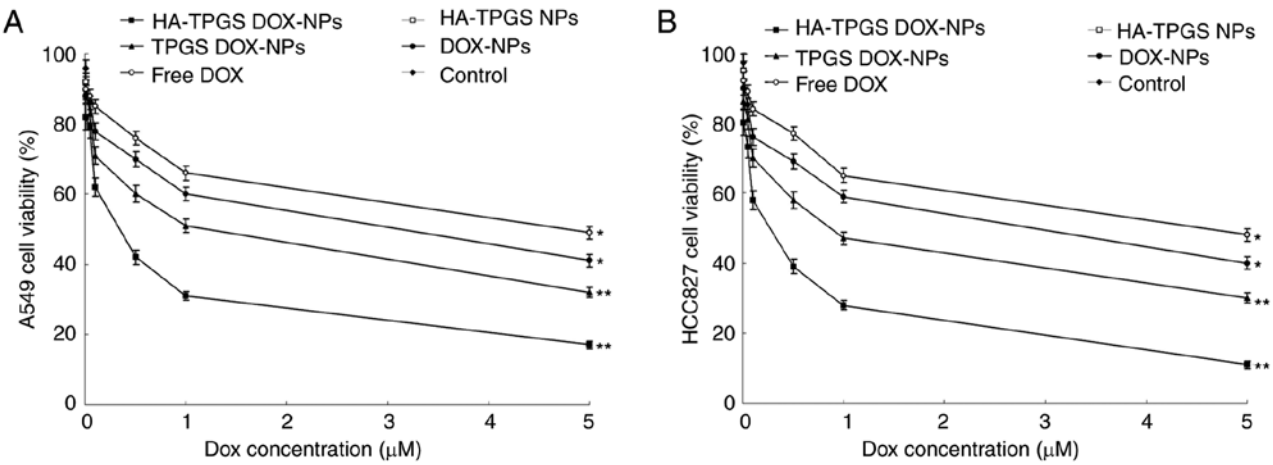

Figure 6. Cell growth inhibition effects of NPs on (A) A549 and (B) HCC827 cells assessed by an MTT assay. In brief, 200 μl A549 and HCC827 cells ($5x10^4$ cells/ml) were seeded into 96-well plates and incubated for 24 h. Various concentrations DOX-loaded NPs and free DOX were added, followed by incubation for 72 h. Values are expressed as the mean ± standard deviation (n=6). Free DOX *P<0.05 vs. the control; DOX-NPs *P<0.05 vs. Free DOX; HA-TPGS DOX-NPs and TPGS DOX-NPs **P<0.01 vs. Free DOX. DOX, doxorubicin; NP, nanoparticle.

the DOX-loaded NP treatment groups exhibited on obvious change. Notably, body weight loss was identified in the free DOX treatment, drug-free NPs and saline control groups.

Discussion

Prodrugs are widely used for targeted delivery of therapeutics to cancer cells (33). Compared with the free active drug, prodrugs may feature a change in the physicochemical nature of the drug and may achieve a marked diversity for cancer therapy. In the present study, the TPGS-S-S-DOX prodrug was constructed for the preparation of NPs (34). Glutathione-sensitive TPGS-S-S-DOX conjugate was designed, synthesized and characterized. First, TPGS-S-S-GA was synthesized by EDC chemistry to conjugate TPGS with S-S and GA. Subsequently, DOX was conjugated to TPGS-S-S-GA to form

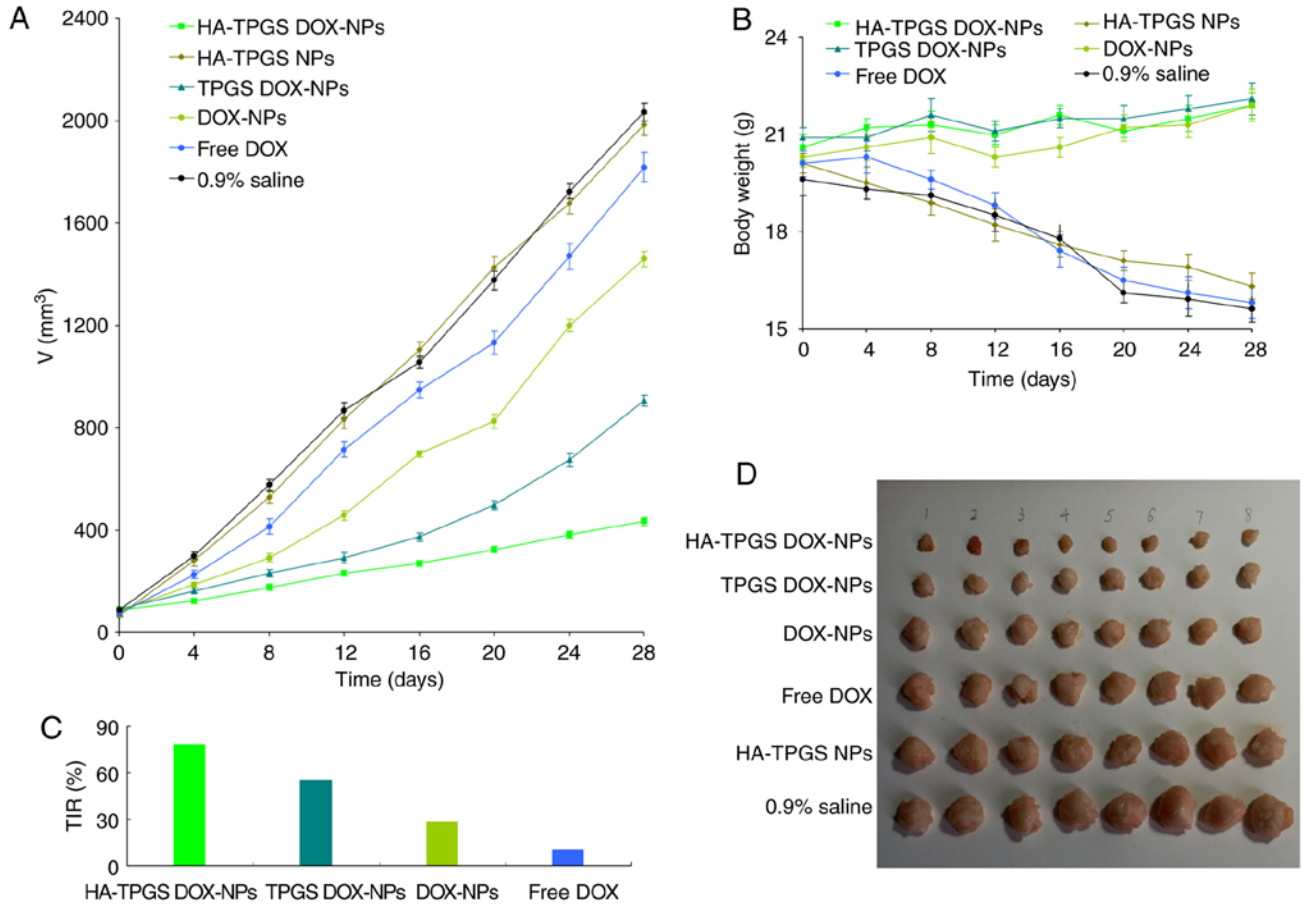

Figure 7. *In vivo* antitumor efficiency evaluated based on the (A) tumor volume, (B) body weight, (C) TIR and (D) images of the tumors. After 1 week, mice with tumors reaching a volume of ~100 mm^3 were randomly divided into 6 groups (8 mice per group) and received 0.2 ml of HA-TPGS DOX-NPs, HA-TPGS NPs, TPGS DOX-NPs, DOX-NPs, free DOX (equivalent DOX concentration, 10 mg/kg) or 0.9% saline solution by intravenous injection via the tail vein on days 0, 4, 8 and 12. The tumor was assessed every 4 days with a Vernier caliper across its two perpendicular diameters. The antitumor efficacy of samples was evaluated by determining the TIR. Images of the tumors were captured at the end of the study. Body weight changes were monitored in order to evaluate the systemic toxicity of the samples. Values are expressed as the mean ± standard deviation (n=8). TIR, tumor inhibition rate; TPGS, D-alpha-tocopheryl polyethylene glycol 1000 succinate; DOX, doxorubicin; HA, hyaluronic acid; NP, nanoparticle.

TPGS-S-S-DOX. The chemical structure of TPGS-S-S-DOX was confirmed using analytic methods.

PLA has been widely used for the preparation of drug delivery systems of anticancer drugs due to its properties of biodegradability, biocompatibility and low toxicity (35). Various methods, including precipitation, emulsion and melting technique, have been used to prepare PLA NP formulations. In the present study, the NPs were self-assembled by using a dialysis method. After preparation, the formulations were characterized. It was observed that the NPs made of PLA displayed a negative charge of -18.2 mV that may be attributed to the negatively charged groups of PLA. In comparison, HA-TPGS DOX-NPs had a higher negative charge of -39.5 mV, which may have arisen from the negatively charged HA added to PLA (36). Electron microscopy techniques, including TEM, may easily provide the size of the NP core. However, due to the low electron density of organic surface ligands, these NPs are difficult to dissolve and DLS is a widely used technique for size determination of NPs in suspension. DLS is able to measure the hydrodynamic diameter of the NPs and determine the dimension of the core plus shell (37). The TEM images indicated that the size of the HA-TPGS DOX-NPs was <200 nm, while DLS suggested a size of 172 nm. PDI may be applied to determine the size range and size distribution of the NPs (38). For polymer-based NP materials, PDI values >0.2 are considered to have a narrow distribution. The reason for the DL of HA-TPGS DOX-NPs being much lower than that of DOX-NPs may be explained by the presence of HA-TPGS increasing the weight of the carriers.

In vitro drug release of the drug-loaded NPs may be controlled by erosion, corrosion and diffusion processes (39). Drug depot effects may be obtained by the carriers, which may lead to the sustained release of hydrophobic drugs. TPGS contains a part of PEG_{1000} (40). PEG-modified NPs may exhibit improved long-term circulating ability compared with the original NPs (41). *In vitro* drug release from NPs exhibits a sustained behavior; mechanistically, this may be attributed to slow degradation of PLA and the release of DOX from NPs depending on drug diffusion, erosion or swelling of PLA (42). Furthermore, the HA-TPGS shell on the outside of the polymer core has a shielding effect and allows for slow and sustained drug release.

Cellular uptake of NPs was quantitatively investigated by flow cytometry (42). The uptake of the NPs by A549 and HCC827 cells increased in a time-dependent manner (43). The cellular uptake efficiency of HA-TPGS DOX-NPs was

significantly higher than that of non-modified NPs; this may be due to the enhanced cancer cell-specific adherence of the HA ligand. HA contained in NP systems may improve the penetration of drugs, which may enhance the efficacy of the drugs, reduce side effects and overcome drug resistance. In the present study, the viability of cells treated with blank HA-TPGS NPs at different concentrations was >85%, indicating low toxicity of the NP system. Low cytotoxicity also indicates biocompatibility of the system, rendering it suitable for administration (44).

The *in vitro* anticancer efficacy of the NPs was evaluated by assessing cell growth inhibition via an MTS assay (45). The highest cytotoxicity among the different NPs achieved with HA-TPGS DOX-NPs may have been due to the HA ligand targeting its receptor on the cancer cells, the enhanced cellular uptake of the NPs and also the enhanced drug release through cleavage of the GSH-responsive bond with the carriers. A DOX dose-dependent anticancer activity was observed in all of the DOX-containing formulations. The results demonstrated that HA-TPGS DOX-NPs had a greater cytotoxic effect on the tumor cells compared with that of non-HA-modified DOX-NPs and free DOX. This may also be attributed to HA having excellent dispersibility in aqueous solution, endowing the NPs with 'stealth' properties (46).

The *in vivo* antitumor efficacy on the NPs was then investigated in a lung cancer-bearing BALB/c mouse model. It was demonstrated that HA-TPGS DOX-NPs had the greatest antitumor effect without any severe adverse effects (body weight loss) (47-49). This result may be attributed to multiple factors. First, the NPs may have utilized the enhanced permeability and retention effect of solid tumors, facilitating targeted delivery of the drugs to the tumor site (50). Furthermore, a similar structure of the lipid shell of the NPs to that of the cell membrane leads to high affinity of the NP systems for the cells, leading to improved drug delivery (51). In addition, the S-S bonds in the prodrug may be rapidly cleaved by intracellular reducing molecules, leading to the release of DOX to the tumor site to achieve intracellular targeting. Finally, HA modification of NPs may provide the best antitumor effect due to the targeting ability of the HA to the receptor on the tumor cells. The results indicated that HA-TPGS DOX-NPs had a more prominent antitumor efficiency than free DOX, DOX-NPs and TPGS DOX-NPs. The safety evaluation results indicated that NPs performed well in the animal model.

In conclusion, HA-TPGS DOX-NPs were constructed and characterized as a lung cancer therapy system for achieving improved efficiency of DOX. It was demonstrated that HA-TPGS DOX-NPs have significant antitumor effects and low systemic toxicity *in vitro* and *in vivo*. The results indicate that HA-TPGS DOX-NPs may be a promising treatment for lung cancer.

Acknowledgements

Not applicable.

Funding

The present study was supported in part by a grant from the 'Thirteen-Five Plan', the Major Program of Nanjing Medical Science and Technique Development Fund (grant no. ZDX16012).

Availability of data and materials

The datasets used during the present study are available from the corresponding author upon reasonable request.

Authors' contributions

YZ, FL, GL and LC conceived and designed the study. GL, LC, CZ, HX, KH, NX and BW performed the experiments. GL, LC, KH, NX and BW wrote the manuscript. YZ, FL, GL and LC reviewed and edited the manuscript. All authors read and approved the manuscript and agree to be accountable for all aspects of the research in ensuring that the accuracy or integrity of any part of the work are appropriately investigated and resolved.

Ethics approval and consent to participate

The animal experiments complied with the Guide for the Care and Use of Laboratory Animals of the National Institutes of Health (publication no. 8023; Bethesda, MD, USA) and approval was obtained from the Institutional Animal Care and Treatment Committee of Southeast University (Nanjing, China).

Patient consent for publication

Not applicable.

Competing interests

The authors declare that they have no competing interests.

References

1. Siegel RL, Miller KD and Jemal A: Cancer statistics, 2017. CA Cancer J Clin 67: 7-30, 2017.
2. Aftab S, Shah A, Nadhman A, Kurbanoglu S, Aysıl Ozkan S, Dionysiou DD, Shukla SS and Aminabhavi TM: Nanomedicine: An effective tool in cancer therapy. Int J Pharm 540: 132-149, 2018.
3. Liu B, Han L, Liu J, Han S, Chen Z and Jiang L: Co-delivery of paclitaxel and TOS-cisplatin via TAT-targeted solid lipid nanoparticles with synergistic antitumor activity against cervical cancer. Int J Nanomedicine 12: 955-968, 2017.
4. Mura S, Bui DT, Couvreur P and Nicolas J: Lipid prodrug nanocarriers in cancer therapy. J Control Release 208: 25-41, 2015.
5. Mi Y, Zhao J and Feng SS: Vitamin E TPGS prodrug micelles for hydrophilic drug delivery with neuroprotective effects. Int J Pharm 438: 98-106, 2012.
6. Anbharasi V, Cao N and Feng SS: Doxorubicin conjugated to D-alpha-tocopheryl polyethylene glycol succinate and folic acid as a prodrug for targeted chemotherapy. J Biomed Mater Res A 94: 730-743, 2010.
7. Xu Z, Liu S, Kang Y and Wang M: Glutathione- and pH-responsive nonporous silica prodrug nanoparticles for controlled release and cancer therapy. Nanoscale 7: 5859-5868, 2015.
8. Tjin CC, Otley KD, Baguley TD, Kurup P, Xu J, Nairn AC, Lombroso PJ and Ellman JA: Glutathione-responsive Selenosulfide prodrugs as a platform strategy for potent and selective mechanism-based inhibition of protein tyrosine phosphatases. ACS Cent Sci 3: 1322-1328, 2017.
9. Wang Y, Liu D, Zheng Q, Zhao Q, Zhang H, Ma Y, Fallon JK, Fu Q, Haynes MT, Lin G, *et al*: Disulfide bond bridge insertion turns hydrophobic anticancer prodrugs into self-assembled nanomedicines. Nano Lett 14: 5577-5583, 2014.
10. Anjukandi P, Dopieralski P, Ribas-Arino J and Marx D: The effect of tensile stress on the conformational free energy landscape of disulfide bonds. PLoS One 9: e108812, 2014.

11. Wang S, Zhang J, Wang Y and Chen M: Hyaluronic acid-coated PEI-PLGA nanoparticles mediated co-delivery of doxorubicin and miR-542-3p for triple negative breast cancer therapy. Nanomedicine 12: 411-420, 2016.
12. Xu W, Qian J, Zhang Y, Suo A, Cui N, Wang J, Yao Y and Wang H: A double-network poly(Nε-acryloyl L-lysine)/hyaluronic acid hydrogel as a mimic of the breast tumor microenvironment. Acta Biomater 33: 131-141, 2016.
13. Duhem N, Danhier F, Pourcelle V, Schumers JM, Bertrand O, Leduff CS, Hoeppener S, Schubert US, Gohy JF, Marchand-Brynaert J and Préat V: Self-assembling doxorubicin-tocopherol succinate prodrug as a new drug delivery system: Synthesis, characterization, and in vitro and in vivo anticancer activity. Bioconjug Chem 25: 72-81, 2014.
14. Zhang Z, Tan S and Feng SS: Vitamin E TPGS as a molecular biomaterial for drug delivery. Biomaterials 33: 4889-4906, 2012.
15. Cao N and Feng SS: Doxorubicin conjugated to D-alpha-tocopheryl polyethylene glycol 1000 succinate (TPGS): Conjugation chemistry, characterization, in vitro and in vivo evaluation. Biomaterials 29: 3856-3865, 2008.
16. Su Z, Chen M, Xiao Y, Sun M, Zong L, Asghar S, Dong M, Li H, Ping Q and Zhang C: ROS-triggered and regenerating anticancer nanosystem: An effective strategy to subdue tumor's multidrug resistance. J Control Release 196: 370-383, 2014.
17. Almeida PV, Shahbazi MA, Mäkilä E, Kaasalainen M, Salonen J, Hirvonen J and Santos HA: Amine-modified hyaluronic acid-functionalized porous silicon nanoparticles for targeting breast cancer tumors. Nanoscale 6: 10377-30387, 2014.
18. Parvani JG, Gujrati MD, Mack MA, Schiemann WP and Lu ZR: Silencing β3 integrin by targeted ECO/siRNA nanoparticles inhibits EMT and metastasis of triple-negative breast cancer. Cancer Res 75: 2316-2325, 2015.
19. Shen W, Liu W, Yang H, Zhang P, Xiao C and Chen X: A glutathione-responsive sulfur dioxide polymer prodrug as a nanocarrier for combating drug-resistance in cancer chemotherapy. Biomaterials 178: 706-719, 2018.
20. Nguyen CT, Tran TH, Amiji M, Lu X and Kasi RM: Redox-sensitive nanoparticles from amphiphilic cholesterol-based block copolymers for enhanced tumor intracellular release of doxorubicin. Nanomedicine 11: 2071-2082, 2015.
21. Liu K, Chen W, Yang T, Wen B, Ding D, Keidar M, Tang J and Zhang W: Paclitaxel and quercetin nanoparticles co-loaded in microspheres to prolong retention time for pulmonary drug delivery. Int J Nanomedicine 12: 8239-8255, 20147.
22. Lee JY, Kim JS, Cho HJ and Kim DD: Poly(styrene)-b-poly(DL-lactide) copolymer-based nanoparticles for anticancer drug delivery. Int J Nanomedicine 9: 2803-2813, 2014.
23. Jiang SP, He SN, Li YL, Feng DL, Lu XY, Du YZ, Yu HY, Hu FQ and Yuan H: Preparation and characteristics of lipid nanoemulsion formulations loaded with doxorubicin. Int J Nanomedicine 8: 3141-3150, 2013.
24. Jia Y, Yuan M, Yuan H, Huang X, Sui X, Cui X, Tang F, Peng J, Chen J, Lu S, *et al*: Co-encapsulation of magnetic Fe_3O_4 nanoparticles and doxorubicin into biodegradable PLGA nanocarriers for intratumoral drug delivery. Int J Nanomedicine 7: 1697-1708, 2012.
25. Li S, Wang L, Li N, Liu Y and Su H: Combination lung cancer chemotherapy: Design of a pH-sensitive transferrin-PEG-Hz-lipid conjugate for the co-delivery of docetaxel and baicalin. Biomed Pharmacother 95: 548-555, 2017.
26. Siu FY, Ye S, Lin H and Li S: Galactosylated PLGA nanoparticles for the oral delivery of resveratrol: Enhanced bioavailability and in vitro anti-inflammatory activity. Int J Nanomedicine 13: 4133-4144, 2018.
27. Yan J, Wang Y, Jia Y, Liu S, Tian C, Pan W, Liu X and Wang H: Co-delivery of docetaxel and curcumin prodrug via dual-targeted nanoparticles with synergistic antitumor activity against prostate cancer. Biomed Pharmacother 88: 374-383, 2017.
28. Ruan C, Liu L, Lu Y, Zhang Y, He X, Chen X, Zhang Y, Chen Q, Guo Q, Sun T and Jiang C: Substance P-modified human serum albumin nanoparticles loaded with paclitaxel for targeted therapy of glioma. Acta Pharm Sin B 8: 85-96, 2018.
29. Arab-Bafrani Z, Shahbazi-Gahrouei D, Abbasian M and Fesharaki M: Multiple MTS assay as the alternative method to determine survival fraction of the irradiated HT-29 colon cancer cells. J Med Signals Sens 6: 112-116, 2016.
30. Pedrosa P, Mendes R, Cabral R, Martins LMDRS, Baptista PV and Fernandes AR: Combination of chemotherapy and Au-nanoparticle photothermy in the visible light to tackle doxorubicin resistance in cancer cells. Sci Rep 8: 11429, 2018.
31. Alibolandi M, Ramezani M, Abnous K, Sadeghi F, Atyabi F, Asouri M, Ahmadi AA and Hadizadeh F: In vitro and in vivo evaluation of therapy targeting epithelial-cell adhesion-molecule aptamers for non-small cell lung cancer. J Control Release 209: 88-100, 2015.
32. Kou CH, Han J, Han XL, Zhuang HJ and Zhao ZM: Preparation and characterization of the Adriamycin-loaded amphiphilic chitosan nanoparticles and their application in the treatment of liver cancer. Oncol Lett 14: 7833-7841, 2017.
33. Giang I, Boland EL and Poon GM: Prodrug applications for targeted cancer therapy. AAPS J 16: 899-913, 2014.
34. Tan S and Wang G: Redox-responsive and pH-sensitive nanoparticles enhanced stability and anticancer ability of erlotinib to treat lung cancer in vivo. Drug Des Devel Ther 11: 3519-3529, 2017.
35. Lee BK, Yun Y and Park K: PLA micro- and nano-particles. Adv Drug Deliv Rev 107: 176-191, 2016.
36. Mura S, Hillaireau H, Nicolas J, Le Droumaguet B, Gueutin C, Zanna S, Tsapis N and Fattal E: Influence of surface charge on the potential toxicity of PLGA nanoparticles towards Calu-3 cells. Int J Nanomedicine 6: 2591-2605, 2011.
37. Shang L, Nienhaus K and Nienhaus GU: Engineered nanoparticles interacting with cells: Size matters. J Nanobiotechnology 12: 5, 2014.
38. Danaei M, Dehghankhold M, Ataei S, Hasanzadeh Davarani F, Javanmard R, Dokhani A, Khorasani S and Mozafari MR: Impact of Particle size and polydispersity index on the clinical applications of lipidic nanocarrier systems. Pharmaceutics 10: E57, 2018.
39. Liu J, Cheng H, Han L, Qiang Z, Zhang X, Gao W, Zhao K and Song Y: Synergistic combination therapy of lung cancer using paclitaxel- and triptolide-coloaded lipid-polymer hybrid nanoparticles. Drug Des Devel Ther 12: 3199-3209, 2018.
40. Cheng W, Liang C, Xu L, Liu G, Gao N, Tao W, Luo L, Zuo Y, Wang X, Zhang X, *et al*: TPGS-Functionalized polydopamine-modified mesoporous silica as drug nanocarriers for enhanced lung cancer chemotherapy against multidrug resistance. Small 13, 2017.
41. Rafiei P and Haddadi A: Docetaxel-loaded PLGA and PLGA-PEG nanoparticles for intravenous application: Pharmacokinetics and biodistribution profile. Int J Nanomedicine 12: 935-947, 2017.
42. Nassireslami E and Ajdarzade M: Gold coated superparamagnetic iron oxide nanoparticles as effective nanoparticles to eradicate breast cancer cells via photothermal therapy. Adv Pharm Bull 8: 201-209, 2018.
43. Jiang L, Li X, Liu L and Zhang Q: Cellular uptake mechanism and intracellular fate of hydrophobically modified pullulan nanoparticles. Int J Nanomedicine 8: 1825-1834, 2013.
44. Guo F, Wu J, Wu W, Huang D, Yan Q, Yang Q, Gao Y and Yang G: PEGylated self-assembled enzyme-responsive nanoparticles for effective targeted therapy against lung tumors. J Nanobiotechnology 16: 57, 2018.
45. Schrand AM, Lin JB and Hussain SM: Assessment of cytotoxicity of carbon nanoparticles using 3-(4,5-dimethylthiazol-2-yl)-5-(3-carboxymethoxyphenyl)-2-(4-sulfophenyl)-2H-tetrazolium (MTS) cell viability assay. Methods Mol Biol 906: 395-402, 2012.
46. Garg A, Rai G, Lodhi S, Jain AP and Yadav AK: Hyaluronic acid embedded cellulose acetate phthlate core/shell nanoparticulate carrier of 5-fluorouracil. Int J Biol Macromol 87: 449-459, 2016.
47. Mei L, Fu L, Shi K, Zhang Q, Liu Y, Tang J, Gao H, Zhang Z and He Q: Increased tumor targeted delivery using a multistage liposome system functionalized with RGD, TAT and cleavable PEG. Int J Pharm 468: 26-38, 2014.
48. Dong Z, Guo J, Xing X, Zhang X, Du Y and Lu Q: RGD modified and PEGylated lipid nanoparticles loaded with puerarin: Formulation, characterization and protective effects on acute myocardial ischemia model. Biomed Pharmacother 89: 297-304, 2017.
49. Naeem M, Bae J, Oshi MA, Kim MS, Moon HR, Lee BL, Im E, Jung Y and Yoo JW: Colon-targeted delivery of cyclosporine A using dual-functional Eudragit® FS30D/PLGA nanoparticles ameliorates murine experimental colitis. Int J Nanomedicine 13: 1225-1240, 2018.
50. Hwang H, Jeong HS, Oh PS, Kim M, Lee TK, Kwon J, Kim HS, Lim ST, Sohn MH and Jeong HJ: PEGylated nanoliposomes encapsulating angiogenic peptides improve perfusion defects: Radionuclide imaging-based study. Nucl Med Biol 43: 552-558, 2016.
51. Kim CE, Lim SK and Kim JS: In vivo antitumor effect of cromolyn in PEGylated liposomes for pancreatic cancer. J Control Release 157: 190-195, 2012.